繰返し載荷を受けるコンクリート充填鋼管部材に対する各種解析モデルの解析精度の比較

白, 涌滔
九州大学大学院人間環境学府空間システム専攻博士後期課程

小俵, 慶太
九州大学大学院人間環境学府空間システム専攻修士課程

河野, 昭彦
九州大学大学院人間環境学研究院都市・建築学部門

松尾, 真太朗
九州大学大学院人間環境学研究院都市・建築学部門

https://doi.org/10.15017/26751

出版情報：都市・建築学研究. 20, pp.101-109, 2011-07-15. Faculty of Human-Environment Studies, Kyushu University
バージョン：
権利関係：

都市・建築学研究　九州大学大学院人間環境学研究院紀要　第20号，2011年7月
J. of Architecture and Urban Design, Kyushu University, No.20, pp.101～109, July. 2011

繰返し載荷を受けるコンクリート充填鋼管部材に対する各種解析モデルの解析精度の比較

Analytical Comparison of Various Models for Concrete-Filled Steel Tubular Columns Subjected to Cyclic Loading

白　涌滔*，小俵慶太**，河野昭彦***，松尾真太朗***
Yongtao BAI*, Keita ODAWARA**, Akihiko KAWANO*** and Shintaro MATSUO***

The hysteresis behaviors of circular and square concrete filled steel tubular were analysed and compared with test results. Local buckling and stiffness degradation are considered for steel model, various simplified analytical models of confined concrete are adopted to verify the accuracy of simulations. Comparison results indicate that steel model adopted in analysis program can accurately perform the local buckling and degradation of steel tube. After comparing different types of confined concrete model, the strength degradation of concrete in circular steel tube could be ignored because of high-level confinement effect, while the strength degradation of the concrete in square steel tube should be considered contrarily. Furthermore, the simplified model based on Sakino & Sun's proposal has the best accuracy on predicting the post-peak degradation behavior of square concrete filled steel tubes.

Keywords: *concrete filled steel tubes, beam columns, cyclic loading, constitutive material model, fiber model analysis*
コンクリート充填鋼管、柱-梁部材、繰り返し載荷、材料要素モデル、ファイバモデル解析

1. INTRODUCTION

Concrete filled steel tube structures have been widely applied in practical civil engineering projects like high-rise buildings, bridges and industrial structures. This structural style has excellent strength and ductility performances to resist intensive earthquake motions. Meanwile, finite element method has been verfied to be an efficient way to simulate structural performances. Therefore, establishing an accurate constitutive model of materials will be essential to guarantee the accuracy of analysis results. Nevertheless, the entire material behavior of concrete filled steel tube structures covering the deterioration after peak caused by local failures such as local buckling or concrete crush hasn't been accurately studied yet.

Various constitutive models of concrete have been proposed to accurately define the pre-peak and post-peak behaviors of concrete filled steel tube structures[1)-6)]. Popovics (1973) primarily proposed the constitutive model of confined concrete, which was modified by Mander et al.[1), 2)]. (1988). Sakino & Sun[3, 4)] proposed the empirical formula for computing the constitutive relationship of confined concrete respectively in various sectional steel tubes (2004), and homogenous model has been proposed by Usami et al.[5), 6)] (1998). Experimental researches were also conducted on cyclic behavior of concrete filled steel tube beam-columns[7)-11)].

The aim of this study is to verify accuracy of material models to predict the global behavior of concrete filled steel tubes by adopting fiber model analysis method. Therefore, cyclic behavior of circular and square sectional CFT specimens are compared between test results and analytical results based on the circular CFT tests conducted by A. Elremaily et al.[7)] and Y. Xiao et al.[8)], and square CFT tests conducted by A. Varma et al.[9), 10)] and E. Inai et al.[11)].

2. CONSTITUTIVE MODEL OF MATERIALS

2.1 Steel tube

In order to simulate the local buckling and stiffness degradation of steel tube, Ohi & Akiyama's stress-strain

*　空間システム専攻　博士後期課程
**　空間システム専攻　修士課程
***　都市・建築学部門

model as shown in Fig. 1 is adopted for both circular and square sectional steel tubes.

Where, E_s is Young's modulus of steel; σ_y is the yield stress of steel materials; R_{ini} is the 'R' for the first M&P (Mengotto & Pinto)[12] curve of the skeleton curve which value has been confirmed as 10.0; σ_u is the ultimate stress of steel materials; R_u is the 'R' for the second M&P curve of the skeleton curve; Ψ is factor to move the skeleton curve; ε_{lb} is strain at local buckling; τ_{lb} is the rate of buckling negative slope to Young's modulus; r_{spm} is rate of the post-buckling strength to the buckling strength; τ_{lb2} is rate of the post-buckling negative slope to Young's modulus.

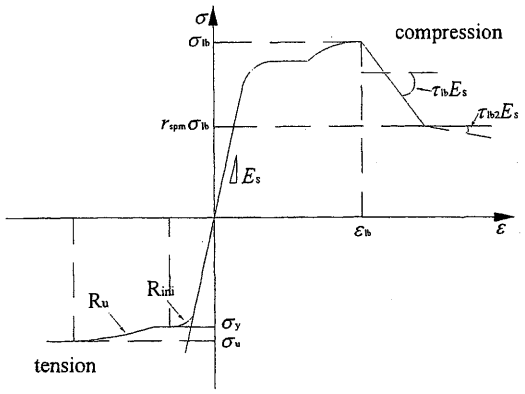

Fig. 1 Ohi & Akiyama's stress-strain model of steel tube

2.2 Confined concrete in Circular CFT

From previous study on circular CFT structures, it is clear that confinement effect of concrete in circular steel tube improves both strength and ductility. Therefore, in order to study behavior before and after buckling happened respectively, the stress-strain model is divided into two parts which respectively is pre-peak and post-peak, and typical simplified model of plain concrete and confined concrete in circular tube are shown in Fig. 2.

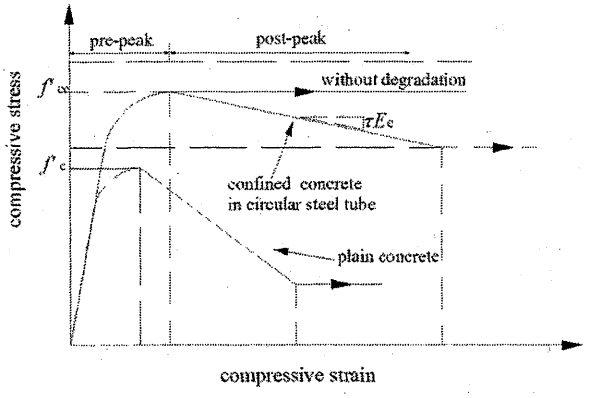

Fig. 2 Simplified stress-strain relationship of the concrete in circular steel tube

2.2.1 Pre-peak behavior

The Popovics's model[1), 2)] is adopted as the stress-strain model of pre-peak part ($0 \le \sigma_c \le f'_{cc}$, $0 \le \varepsilon_c \le \varepsilon_{cc}$), the formulas of constitutive model is shown in Eq.(1), (2). Young's modulus of confined concrete are calculated based on reference[13] as shown in Eq.(3).

$$\sigma_c = f'_{cc} \times \frac{r\left[\varepsilon_c / \varepsilon'_{cc}\right]}{r-1+\left[\varepsilon_c / \varepsilon'_{cc}\right]^r} \tag{1}$$

$$r = \frac{E_c}{E_c - (f'_{cc} / \varepsilon_{cc})} \tag{2}$$

$$E_c = (3.32\sqrt{f'_{cc}} + 6.90) \cdot 10^3 \text{ (MPa)} \tag{3}$$

Besides, Sakino & Sun's proposal[3, 4)] is adopted to define the strength of the confined concrete as shown in Eq.(4), and strain corresponding to confined strength as shown in Eq.(5), (6).

$$f'_{cc} = f'_c(1+1.56\times\frac{\sigma_y}{f'_c}(\frac{D}{t}-2)^{-1}) \tag{4}$$

$$\varepsilon_{cc} = 0.94 f'^{(1/4)}_{cc} \times 10^{-3} \times \begin{cases} 1+4.7(K-1) \\ 3.4+20(K-1) \end{cases} \begin{matrix} K \le 1.5 \\ K > 1.5 \end{matrix} \tag{5}$$

$$K = 1 - k \cdot \alpha_u \cdot 2\frac{\sigma_y}{f'_c}(\frac{D}{t}-2)^{-1} \tag{6}$$

Where, E_c is Young's modulus of confined concrete; D and t are diameter and thickness of steel tube, respectively; σ_c and ε_c are stress and strain value of confined concrete in pre-peak period, respectively; f'_{cc} and ε_{cc} are peak stress and corresponding strain, respectively; E_c is Young's modulus; σ_y is yield stress of steel tube; k is confinement coefficient=4.1 (Richart et al.)[14]; α_u is normalized hoop stress in circular steel tube at ultimate load=-0.19[15].

2.2.2 Post-peak behavior

Researchers[3)~6)] proposed various empirical equations on the post-peak behavior of confined concrete in circular CFT. While, given the circular steel tubular provide considerable confinement effect on core concrete, the stiffness degradation after peak are ignored in analysis program which is expressed as horizontal line after peak.

2.3 Square CFT

The confinement effect of concrete in rectangular CFT is quite different from circular CFT, the stress-strain model is shown in Fig. 3. Rectangular steel tube rarely improves the strength of confined concrete, while it obviously improves the degradation stiffness of confined concrete compared with plain concrete.

2.3.1 Pre-peak behavior

The pre-peak behavior of the confined concrete in square CFT is similar to circular CFT as shown in equation (1)-(3) which is proposed by Popovics[1, 2)]. The confined strength of concrete and strain corresponding to confined strength are calculated as Eq. (7)-(9).

$$f_{cc}^{'} = \gamma_c f_c^{'} \quad (7)$$

$$\gamma_c = 1.67 \times D^{'(-0.112)} \quad (8)$$

$$\varepsilon_{cc}^{'} = 0.94 f_{cc}^{'(1/4)} \times 10^{-3} \quad (9)$$

Where D' is the diameter of the circularity which has the same area with the square section.

2.3.2 Post-peak behavior

As shown in Fig. 3, the post-peak model is simplified into linear relationship, the degradation modulus τE_c of the post-peak period could be computed by two points of (f'_{cc}, ε'_{cc}) and ($\alpha f'_{cc}$, ε'_{cu}) as in Eq. (10). Therefore, the coefficients of α and ε'_{cu} are required to be defined.

$$\tau E_c = \frac{f_{cc}^{'} - \alpha f_{cc}^{'}}{\varepsilon_{cu}^{'} - \varepsilon_{cc}^{'}} \quad (10)$$

The simplified post-peak model is calculated based on Sakino & Sun proposal[3, 4] as shown in Table 1. Meanwhile,

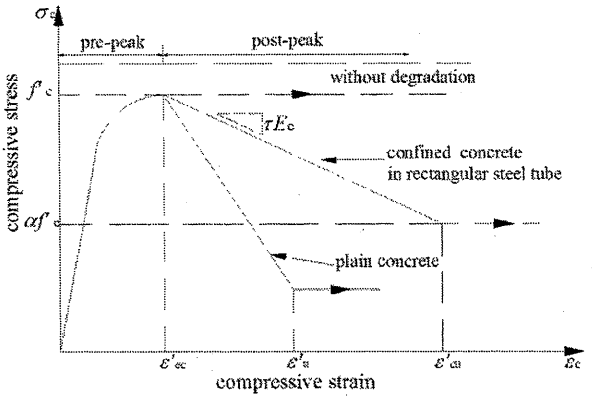

Fig. 3 Simplified stress-strain relationship of the concrete in square section steel tube

the model of Usami et al.[5, 6] is also adopted in analysis program to verify the accuracy of simplified model mentioned above which is shown in Table 1. Where, v is poisson ratio of steel which is equal to 0.3.

3. COMPARISON BETWEEN TEST & ANALYSIS

3.1 Circular CFT beam columns

Due to strong confinement effect of core concrete from circular steel tube, degradation stiffness after peak is ignored in analysis model. Concrete and steel tube models are established as in 2.1, 2.2. Test matrix of specimens and comparison of moment capacity are shown in Table 2, 3. Loading procedure for test and fiber model analysis[16] is cyclic horizontal loading with constant axial loading as shown in Fig.4. Analytical results and tests results[7, 8] of hysteresis behavior are compared and shown in Fig.5~7.

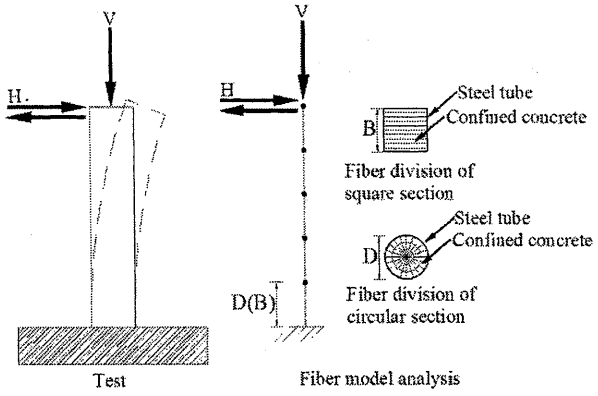

Fig. 4 Loading procedure of test and fiber model analysis

Table 1 Parameters for the post-peak behavior of concrete in square CFT

Parameters	No degradation	Simplified model based on Sakino & Sun's proposal[16]	Model of Usami et al.[4, 5]
τE_c	0	$\tau E_c = \frac{f_{cc}^{'} - \alpha f_{cc}^{'}}{\varepsilon_{cu}^{'} - \varepsilon_{cc}^{'}}$ $\alpha = 1 - \frac{1}{W}$ $W = 1.50 - 17.1\times10^{-3} f_{cc}^{'} + 2.39\sqrt{2f_y(\frac{B}{T}-1)(\frac{B}{T}-2)^{-3}}$	$\tau E_c = -\left\{\begin{matrix} 0 \\ 23400 \times R\frac{f_c^{'}}{f_y} - 91.26 \end{matrix}\right\} \begin{matrix} R\frac{f_c^{'}}{f_y} \le 0.0039 \\ R\frac{f_c^{'}}{f_y} > 0.0039 \end{matrix}$ $R = \frac{B}{t}\sqrt{\frac{3(1-\nu^2)}{\pi^2}}\sqrt{\frac{f_y}{E_s}} = 0.53\frac{B}{t}\sqrt{\frac{f_y}{E_s}}$
α	1	$\alpha = 1 - \frac{1}{W}$	$\alpha = 1 - \frac{\tau E_c \times (\varepsilon_{cc}^{'} - \varepsilon_{cu}^{'})}{f_c^{'}}$
ε'_{cu}	N/A	ε'_{cu}=0.015	$\varepsilon_{cu}^{'} = \left\{\begin{matrix} 0.04 \\ 14.50\left[R\frac{f_c^{'}}{f_y}\right]^2 - 2.4R\frac{f_c^{'}}{f_y} + 0.116 \\ 0.018 \end{matrix}\right\} \begin{matrix} R\frac{f_c^{'}}{f_y} \le 0.042 \\ 0.042 < R\frac{f_c^{'}}{f_y} < 0.073 \\ R\frac{f_c^{'}}{f_y} \ge 0.073 \end{matrix}$

Table 2 Matrix of the circular sectional CFT specimens

References	Specimens NO.	Geometrical properties				Material properties		Axial load level
		D/t	t (mm)	D	L (mm)	f_c (MPa)	f_y (MPa)	P/P_0
A. Elremaily & A. Azizinamini[7]	CFT-1	51	6.4	326.4	914	100	372	0.33
	CFT-5	51	6.4	326.4		40		0.4
	CFT-6	51	6.4	326.4		70		0.32
	CFT-2	34	9.5	323		104		0.2
	CFT-3	34	9.5	323		104		0.4
	CFT-4	34	9.5	323		40		0.42
Yan Xiao et al.[8]	C1-CFT3	112	3	336	1500	39.1	303	0.47

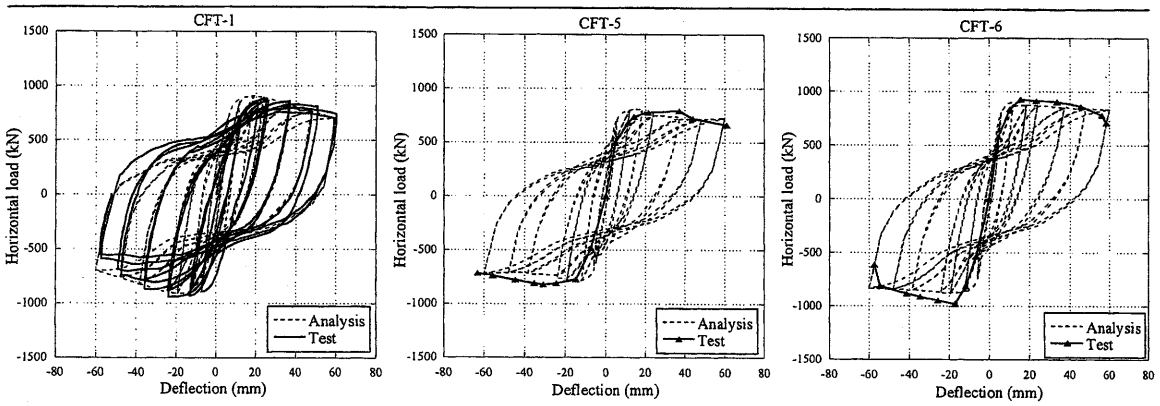

(a) CFT-1 (f'_c=100MPa) (b) CFT-5 (f'_c=40MPa) (c) CFT-6 (f'_c=70MPa)

Fig. 5 Specimens with the width-thickness ratio of 51

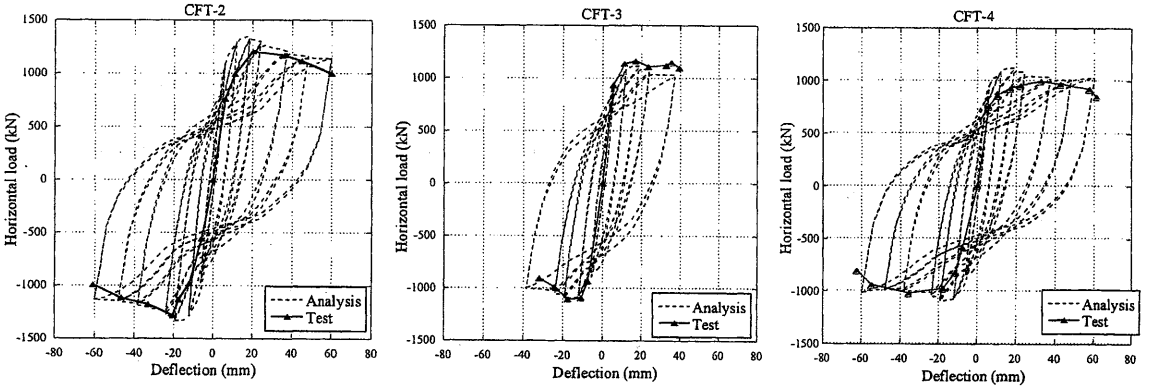

(a) CFT-2 (f'_c=104MPa) (b) CFT-3 (f'_c=104MPa) (c) CFT-4 (f'_c=40MPa)

Fig. 6 Specimens with the width-thickness ratio of 34

Table 3 Moment capacity comparison

Name of specimens	Moment capacity			M_{exp} /M_{ana}
	Test (kN.m)	LRFD (kN.m)	Analysis (kN.m)	
CFT-1	542.4	283.7	518.2	1.05
CFT-5	450.9	170.5	461.1	0.98
CFT-6	511.9	254.6	540.9	0.95
CFT-2	617.0	455.3	653.4	0.94
CFT-3	663.3	281.7	634.8	1.04
CFT-4	544.7	205.1	626.9	0.87

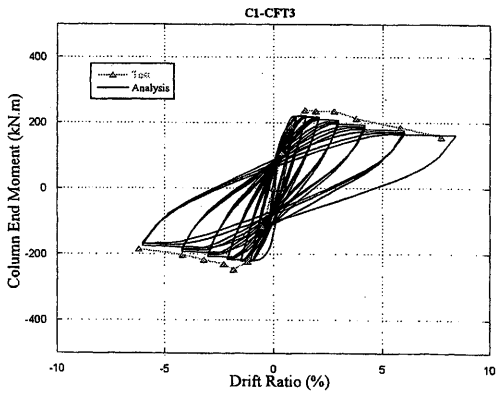

Fig. 7 Comparison of moment versus drift-ratio between tests envelop and analysis hysteresis

Fig. 5~6 shows the comparison of analytical and test horizontal load-deflection curves with different diameter-thickness ratio and concrete strength. It is observed that predicted curves mainly have good agreement with test results by using degradation model of steel and no-degradation model of confined concrete. Besides, moment capacity of specimens[7] are calculated and compared with test and LRFD code results as shown in Table 3.

As shown in Fig. 7, analytical result of C1-CFT3 has accurate prediction with test results by adopting material model as mentioned in 2.1, 2.2.

3.2 Square CFT

Square CFT beam-columns are analysed and compared with cyclic horizontal loading (constant axial loading) tests conducted by Varma, Ricles et al.[9), 10)] and E. Inai et al.[11)]. Different material models of steel (no degradation in Fig. 8(a); Ohi &Akiyama's model with local buckling and degradation in Fig. 8 (b-d), Fig. 9-11); concrete (no degradation in Fig. 8-11 (b); model based on Sakino & Sun's proposal in Fig. 8(d), 9-11(a); model based on the proposal of Usami et al. in Fig. 8(c), 9-11(c)) are adopted in analysis program to verify the simulation accuracy of each model.

Test matrix of specimens is shown in Table 4, and comparison results of horizontal loading versus displacement hysteresis curves are respectively shown in Fig. 8~12.

Table 4 Test matrix with specimens

Authors	Specimen	f_y	f'_c	Nominal B/t ratio	Thickness (mm)	Test length (m)	P/P_0
Varma, Ricles et al.[9, 10)]	CBC-32-80-10	600	110	32	8.9	1.5	0.1
	CBC-32-80-20	600	110	32	8.9	1.5	0.2
	CBC-48-80-10	660	110	48	6.1	1.5	0.11
	CBC-48-80-20	660	110	48	6.1	1.5	0.22
E. Inai et al.[11)]	SR4-A-4-C	295	35.5–42.4	35	6.0	1.26	0.4
	SR4-A-9-C	295	84.5–94.5	35	6.0	1.26	0.4
	SR4-C-4-C	276	35.5–42.4	47	4.5	1.26	0.4
	SR4-C-9-C	276	84.5–94.5	47	4.5	1.26	0.4

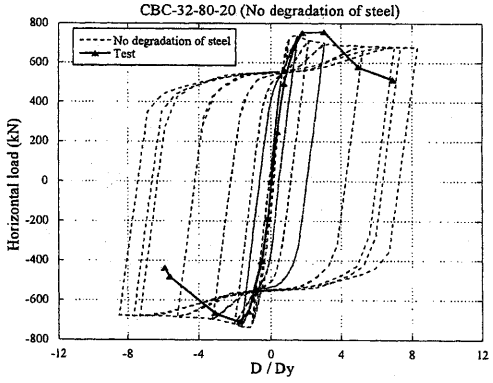

(a) No post-peak degradation of steel

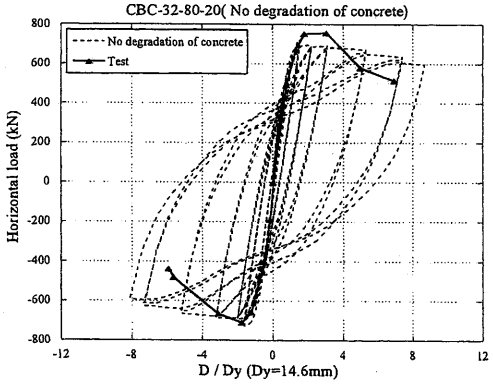

(b) No post-peak degradation of concrete

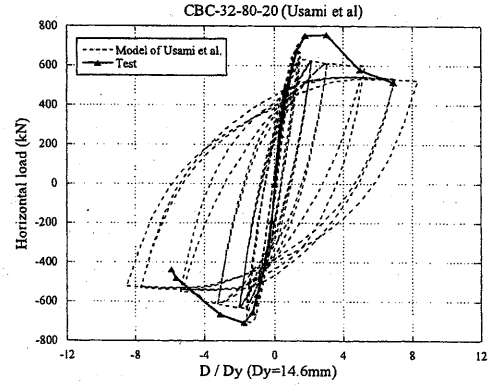

(c) Model of Usami at al.

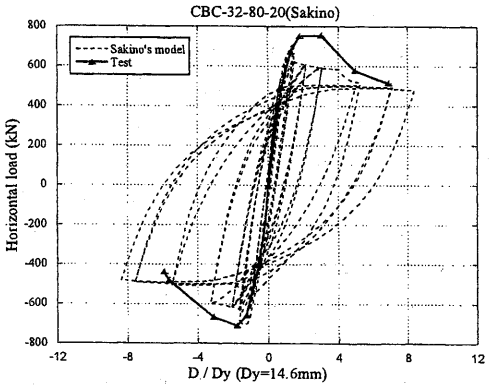

(d) Sakino & Sun's model

Fig. 8 Comparison of the horizontal load-displacement responses the CBC-32-80-20

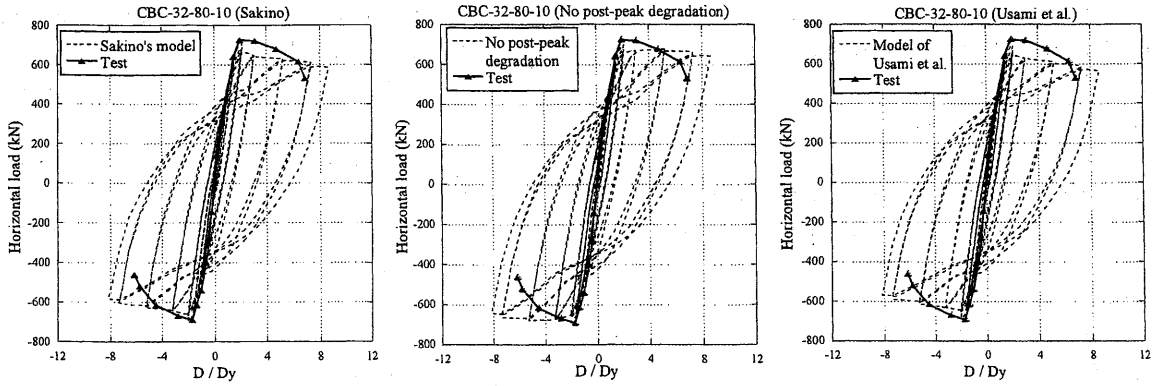

(a) Sakino's model (b) No post-peak degradation (c) Model of Usami at al.

Fig. 9 Comparison of the horizontal load-displacement responses the CBC-32-80-10

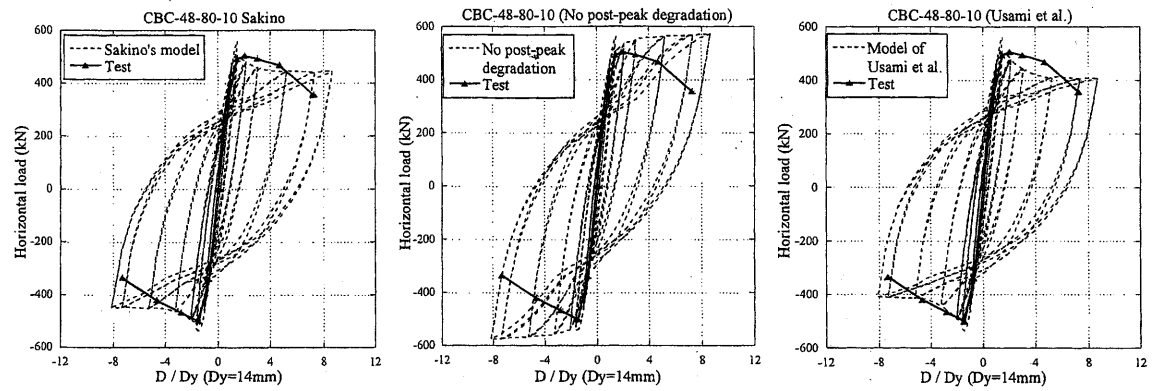

(a) Sakino's model (b) No post-peak degradation (c) Model of Usami at al.

Fig. 10 Comparison of the horizontal load-displacement responses the CBC-48-80-10

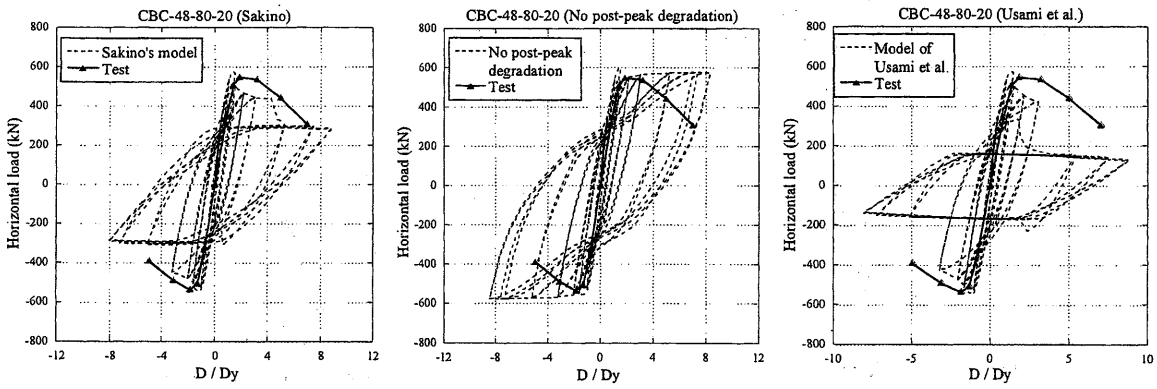

(a) Sakino's model (b) No post-peak degradation (c) Model of Usami at al.

Fig. 11 Comparison of the horizontal load-displacement responses CBC-48-80-20

As shown in Fig. 8 (a), it is observed that ignoring the material degradation of steel mainly lead to overestimation of hysteresis area and gradient in post-peak region. As shown in Fig. 8-11(b) Ignoring of the concrete material degradation will only reduce the gradient in post-peak region, which results in the overestimate of member's after peak behavior. Therefore, post-peak degradations of steel and concrete as shown in Fig. 1-3 are essential to be considered, and concrete model based on the proposals of Sakino and Sun's proposal and model of Usami et al. have better agreement with test results.

According to the comparison results in Fig. 8~10, concrete models based on Sakino & Sun's proposal and proposal of Usami et al. have nearly accurate predictions, while when the width-thickness ratio becomes larger and axial load level keeps high, the former model has more accurate results as shown in Fig. 10. Specimens[11] are only analysed by using simplified model based on Sakino & Sun's proposal and Ohi &Akiyama's model of steel with local buckling and degradation as shown in Fig. 12.

In Fig. 12, the analytical results have acceptable underestimate compared with test curves, and analytical

results can accurately simulate the stiffness of pre-peak and post-peak periods. Besides, the moment capacity of prediction values and test values are SR4A4C (M_{ua}=166.83kNm, M_{ue}=187kNm); SR4A9C (M_{ua}=213kNm, M_{ue}=225kNm); SR4C4C (M_{ua}=128kNm, M_{ue}=151kNm); SR4C9C (M_{ua}=172kNm, M_{ue}=202kNm); respectively. The corresponding ratio between test and analytical results (M_{ue}/M_{ua}) are 1.12, 1.06, 1.18, 1.17. It indicates that analysis program in this comparison is creditable and stable to simulate square CFT structures.

3.3 Degradation modulus (τE_c)

Post-peak degradation of represents the behavior after CFT structures happening local buckling, which also express the ductility performance after structure achieving strength. The values of degradation gradient are derived from the peak-point of local-buckling happened and peak point of ending circle from hysteresis curves in Fig. 8-10 (Ohi &Akiyama's model of steel with local buckling & degradation; various degradation models of concrete), and connecting them together to form descending curve after peak as presented in Fig. 13~15.

From Fig. 13-15, it is observed that ignoring degradation of concrete always overestimate the post-peak behavior of square CFT members. The other two Models with considering the degradation of concrete exhibit homogenous results and are relatively accurate to simulate post-peak behavior of square CFT.

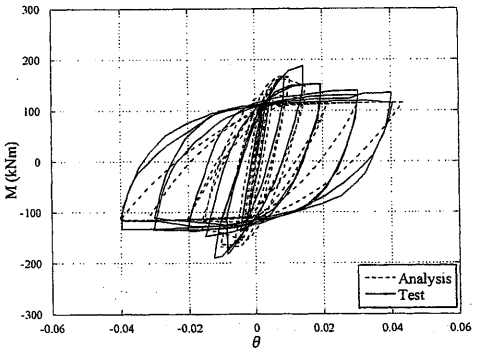

(a) SR4A4C

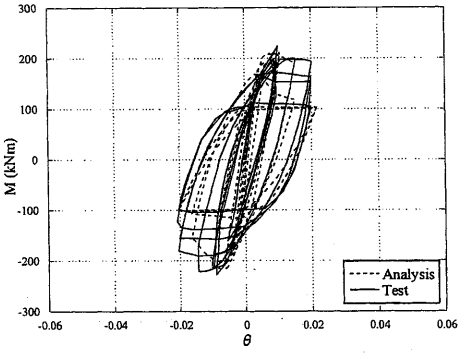

(b) SR4A9C

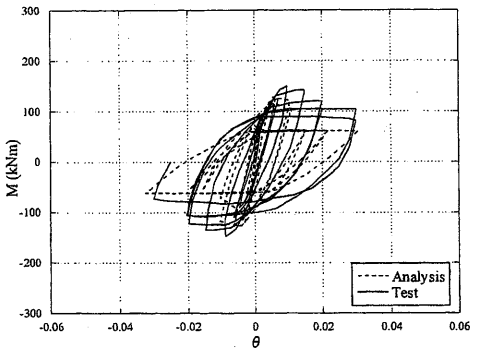

(c) SR4C4C

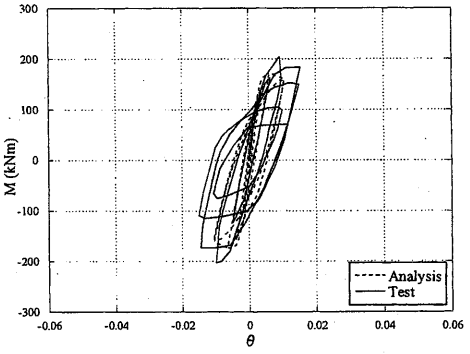

(d) SR4C9C

Fig. 12 Hysteresis comparison of test and analytical results

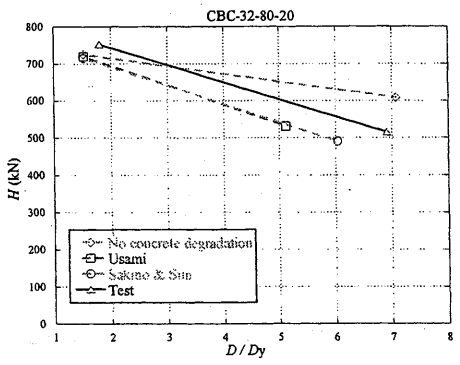

(a) Positive direction

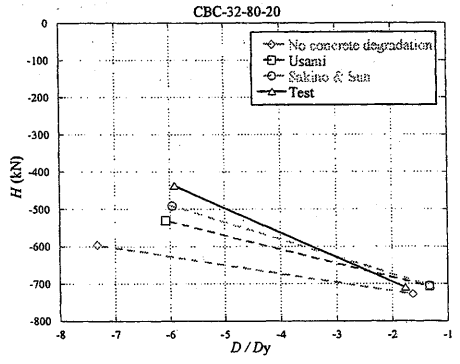

(b) Negative direction

Fig. 13 Comparison of the descending slope of CBC-32-80-20

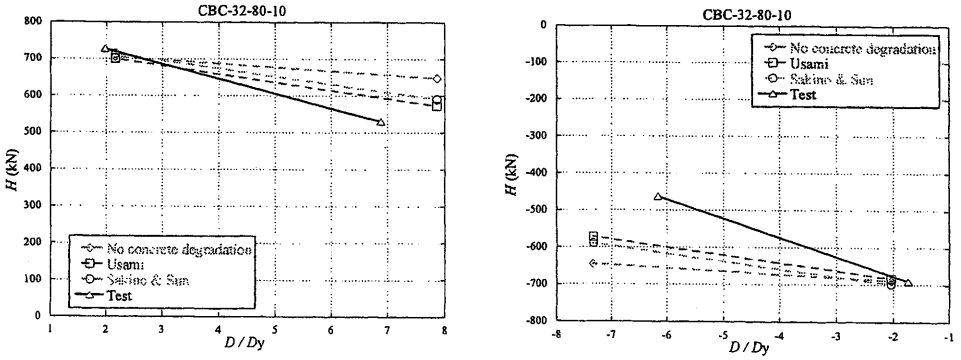

(a) Positive direction (b) Negative direction

Fig. 14 Comparison of the descending slope of CBC-32-80-10

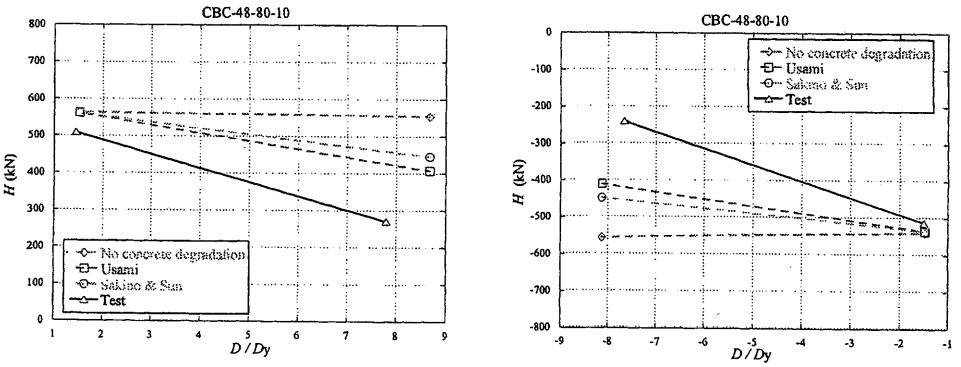

(a) Positive direction (b) Negative direction

Fig. 15 Comparison of the descending slope of CBC-48-80-10

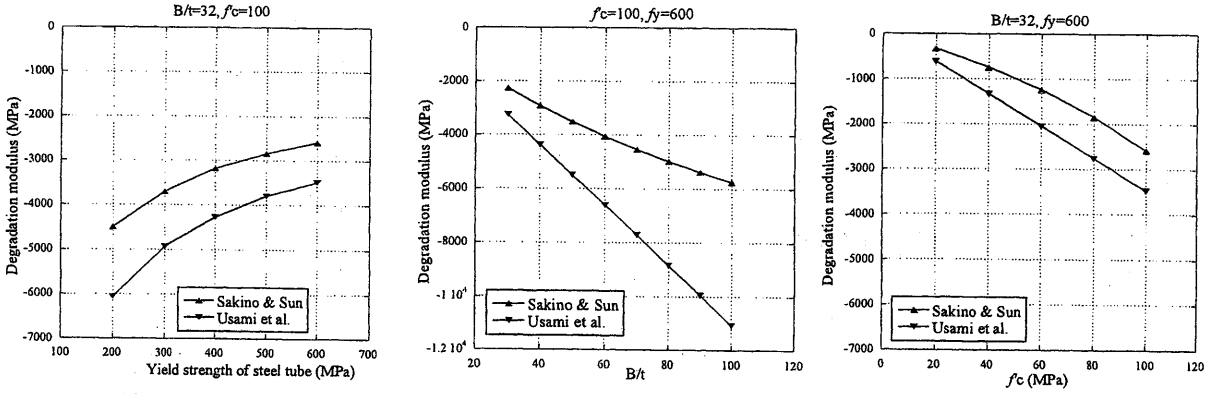

(a) Considering f_y (b) Considering B/t (c) Considering f'_c

Fig. 16 Comparison of the post-peak gradients of the confined concrete in square CFT

Thus, the post-peak gradient of these two models as shown in Table 1 are calculated and compared based on the parameters of cylinder strength of concrete (f'_c), the yield strength of steel (f_y) and the width-thickness ratio of steel tubes (B/t). Comparison results are shown in Fig. 16.

As shown in Fig. 16, the comparisons indicate that when the concrete strength or width-thickness ratio become smaller, the above two models would exhibit better agreement on degradation modulus when the yield strength of steel becomes larger, the degradation modulus of above two models basically kept the same ratio, (ratio of τE_c between Sakino & Sun's model and model of Usami at al. changes 0.52-0.7 (B/t: 100-30); 0.54-0.74 (f'_c: 100-20); 0.74-0.75 (f_y: 200-600)). Besides, considering the comparisons between analysis and tests, simplified model based on Sakino & Sun's proposal exhibits more accurate predictions on degradation gradient than model based on the proposal of Usami et al., because the later one will show too conservative results when parameters change.

4. CONCLUSIONS

An analytical comparison of circular and square CFT beam-columns under cyclic loadings (constant axial loadings, cyclic horizontal loadings) between FEM simulation and test is conducted to verify the prediction

accuracy of different material models. Conclusions based on analytical investigation can be summarized as follows.

1. The fiber model analysis adopted in this study is accurate and reliable to simulate CFT beam-columns and other homogenous structures, according to the global performances of analytical results.

2. Based on the comparison results of circular CFT beam-columns, confined concrete exhibits high level confinement by circular steel tube, the comparison results have good agreement by ignoring the strength degradation of concrete after peak.

3. Since the behavior of confined concrete in square steel tube is improved not as much as circular CFT, the stiffness degradation should not be ignored. Otherwise, the post-peak behavior will be overestimated according to the prediction results.

4. For the post-peak model of confined concrete in square CFT, Simplified models based on different proposals have different analytical results. Analytical results by adopting simplified model indicate that Sakino & Sun's proposal can accurately predict the behavior of confined concrete in square CFT, while the proposal of Usami et al may generate underestimation of the post-peak behavior of confined concrete in square CFT.

REFERENCES

1) Popovics S: A Numerical Approach to the Complete Stress–Strain Curves for Concrete. Cement Concrete Researches, Vol. 3, No. 5, pp. 583-99, 1973.
2) Mander J. B, Priestly J. N and Park R: Theoretical Stress–Strain Model for Confined Concrete, Journal of Structural Engineering, Vol. 114, No. 8, pp. 1804-26, 1988.
3) Sakino K. and Sun Y: Stress–Strain Curve of Concrete Confined by Rectilinear Hoop, Journal of Structural and Construction Engineering, No. 461, pp. 95–104, 1994.
4) Kenji Sakino, Hiroyuki Nakahara, Shosuke Morino, and Isao Nishiyama: Behavior of Centrally Loaded Concrete-Filled Steel-Tube Short Columns, Journal of Structural Engineering, Vol. 130, No. 2, pp. 180-8, 2004.
5) T. Usami, H.B. Ge: Cyclic Behaviour of Thin-Walled Steel Structures-Numerical Analysis, Thin-walled Structures, No. 32, pp. 41–80, 1998.
6) K.A.S. Susantha, Hanbin Ge and Tsutomu Usami: Uniaxial Stress–Strain Relationship of Concrete Confined by Various Shaped Steel Tubes, Engineering Structures, No. 23, pp. 1331–47, 2001.
7) Ahmed Elremaily, Atorod Azizinamini: Behavior and strength of circular concrete-filled tube columns, Journal of Constructional Steel Research, No. 58, pp. 1567-91, 2002.
8) Yan Xiao, Wenhui He, Kang-kyu Choi: Confined Concrete-Filled Tubular Columns, Journal of Structural Engineering, Vol. 131, No. 3, pp. 488-197, 2005.
9) A.H. Varma, James M. Ricles, Richard Sause, Le-Wu Lu: Seismic Behavior and Design of High-Strength Square Concrete-Filled Steel Tube Beam Columns, Journal of Structural Engineering, Vol. 130, No. 2, pp. 169-179, 2004.
10) A.H. Varma, James M. Ricles, Richard Sause, Le-Wu Lu: Seismic Behavior and Modeling of High-Strength Composite Concrete-Filled Steel Tube (CFT) Beam-Columns, Journal of Constructional Steel Research, No. 58, pp. 725-758, 2002.
11) Eiichi Inai, Akiyoshi Mukai, Makoto Kai, Hiroyoshi Tokinoya, Toshiyuki Fukumoto and Koji Mori: Behavior of Concrete-Filled Steel Tube Beam Columns, Journal of Structural Engineering, Vol. 130, No. 2, pp. 189-202, 2004.
12) Mengotto M., Pinto P. E: Method of Analysis for Cyclically Loaded R. C. Frames Including Changes in Geometry and Non-elastic Behaviour of Elements Under Combined Normal Force and Bending, IABSE Congress Reports of the Working Commission, Band 13, 1973.
13) Martinez et al.: Spirally Reinforced High-Strength Concrete Columns, ACI Journal, Vol. 81, No. 35, pp. 431-42, 1984.
14) Richart F. E., Brandzaeg A. and Brown R. L: The Failure of Plain and Spirally Reinforced Concrete in Compression, Univ. Illinois, Engineering Experimental Station, Urbana, Ill, Bulletin No. 190, 1929.
15) Architectural Institute of Japan (AIJ): Recommendations for Design and Construction of Concrete Filled Steel Tubular Structures, Tokyo, 2008.
16) A. Kawano, K. Sakino: Seismic Resistance of CFT Trusses, Engineering Structures, Vol. 25, pp. 607-19, 2003.

（受理：平成23年6月2日）